https://doi.org/10.3311/PPch.12959

Periodica Polytechnica Chemical Engineering, 64(1), pp. 61–74, 2020

Mg and La Co-doped ZnO Nanoparticles Prepared by Sol–gel Method: Synthesis, Characterization and Photocatalytic Activity

Behnam Khanizadeh[1], Morteza Khosravi[1], Mohammad A. Behnajady[2*], Ali Shamel[3], Behrouz Vahid[4]

[1] Department of Applied Chemistry, North Tehran Branch, Islamic Azad University, Tehran 1651153311, Iran
[2] Department of Chemistry, Tabriz Branch, Islamic Azad University, Tabriz 5157944533, Iran
[3] Department of Chemistry, Ardabil Branch, Islamic Azad University, Ardabil 5615731567, Iran
[4] Department of Chemical Engineering, Tabriz Branch, Islamic Azad University, Tabriz 5157944533, Iran
* Corresponding author, e-mail: behnajady@iaut.ac.ir

Received: 07 August 2018, Accepted: 02 October 2018, Published online: 23 April 2019

Abstract

In this study, La and Mg doped, and co-doped ZnO nanoparticles were prepared using the sol-gel method. The prepared samples were characterized by X-ray diffraction (XRD), field emission scanning electron microscopy (FESEM), energy dispersive X-ray spectroscopy (EDX), transmission electron microscopy (TEM), UV-Vis diffuse reflectance spectroscopy (DRS), and N_2 physisorption techniques. The XRD results indicated that the prepared nanoparticles can be well adopted by the hexagonal wurtzite structure crystal and there are no second impurity peaks. Studies of the FESEM, EDX and TEM have shown that the samples have uniform spherical-like morphology with a homogenous distribution. The incorporation of La and Mg into the ZnO lattice had no effect on the morphology of the nanoparticles, but a reduction in the size of the grains (≈ 14 nm to ≈ 7 nm) was observed due to the insertion of these ions. The results of N_2 physisorption indicated that there was an increase in BET surface area and pore volume for doped and co-doped samples. The results of DRS showed an increase in band gap energy and a blue shift at the absorption edge for doped and co-doped samples. The photocatalytic activity of the prepared catalysts was evaluated in the removal of RhB under UVA irradiation. The results showed that Mg5%-La5%/ZnO had the highest photoactivity (91.18 %) among all samples.

Keywords

heterogeneous photocatalysis, co-doped ZnO, photocatalytic activity, Rhodamine B, sol-gel method

1 Introduction

The vast consumption of water in various industries, particularly in color production, leads to remarkable wastewater which can pollute the environment. Hence, for preventing water pollution, it is necessary to remove organic compounds before they are discharged into wastewater [1-8]. Since 1 to 20 % of the overall produced dyes are released into the environment [2, 8, 9], this procedure is considered as a notable concern and an international problem for human beings [10]. Due to the production of toxic metabolites [2], especially aromatic amines [9], these pollutants are regarded as poisonous [5, 9, 11, 12], resistant to biological treatment [2, 5, 11], stable in environment [2] and carcinogenic [12, 13]. The presence of organic materials in wastewater consumes dissolved oxygen [2, 7], reduces the process of photosynthesis, and decreases the solubility of gases [7, 12]. Adsorption, ultrafiltration, reverse osmosis, coagulation, sedimentation, and ozone treatment are assumed as traditional treatment methods which have disadvantages such as high costs, production of toxic sludge, ineffective degradation and low mineralization of organic dyes, nondestructive decolorization, producing secondary pollution and high treatment time [2, 5, 7, 12-16]. New development in water treatment has led to the technology of Advanced Oxidation Processes (AOPs) which are widely used for mineralizing toxic pollutants and a variety of recalcitrant organics in wastewaters [2, 3, 7, 8, 16-20]. Given different AOPs, heterogeneous photocatalysis is regarded as an effective and promising technique [4, 12, 13].

In the heterogeneous photocatalysis, a semiconductor photocatalyst is excited by UV irradiation which forms electron-hole pairs. Hydroxyl radicals and reactive oxygen species (ROS) with high oxidation potential are produced

Cite this article as: Khanizadeh, B., Khosravi, M., Behnajady, M. A., Shamel, A., Vahid, B. "Mg and La Co-doped ZnO Nanoparticles Prepared by Sol–gel Method: Synthesis, Characterization and Photocatalytic Activity", Periodica Polytechnica Chemical Engineering, 64(1), pp. 61–74, 2020. https://doi.org/10.3311/PPch.12959

subsequent reactions. These species are mainly responsible for oxidizing organic pollutants, especially aromatic rings.

Notable instances of photocatalysts are ZnO, TiO_2, Zn_2SnO_4, WO_3, V_2O_5, CdS, Cu_2O, W_2O_5, Fe_2O_3, ZnS, ZrO_2, CeO_2 and etc. [1, 13, 19, 21, 22]. Significant merits of ZnO are as follows: i) heterogeneous photocatalyst [9, 23-35], ii) more efficiency than TiO_2 under UV light [1, 7, 20, 22, 35, 36], iii) high transformation of organic component [37], iv) high activity in removing organic contaminants [23], v) high luminescent activity [35], vi) high activity surface due to large number of active sites [1] and vii) absorption of an extensive range of UV spectrum [22]. However, ZnO has low quantum efficiency due to high recombination electron-hole pairs [5, 7]. With respect to UV irradiation on ZnO surface, charge separation should be very fast after the generation of electron-hole pairs for delaying the recombination process [9]. The recombination rate of the electron-hole pairs can be reduced by coupling with other metal oxides [38-41] and also by doping and co-doping of metal and nonmetal ions into the photocatalyst lattice [4, 19, 22, 26, 29, 30, 34-36, 42-53]. The sol-gel method is a very versatile process for homogeneous doping or co-doping of ions into the ZnO lattice [54, 55].

Behnajady et al. [56], noted a superior photocatalytic activity for Mg-doped TiO_2 in comparison with un-doped TiO_2 for the degradation of C.I. Acid Red 27. The highest photocatalytic activity of Mg-doped TiO_2 in comparison with other M-doped TiO_2 catalysts (M=Fe, Co, Ce, Cr, Mn, Ni and Ag ions), was defined by Feng et al. for the degradation of Rhodamine B in an aqueous solution [57]. Wang et al. [58], informed an improved photocatalytic activity for Ag/ZnO-SnO_2 photocatalyst in compared with pure ZnO-SnO_2 in degradation MO. In recent years, some studies have been done on preparing co-doped ZnO such as, Al-Sn/ZnO, Li-Mg/ZnO, Gd-ZnO:Al, Al-Na/ZnO, Mn-Co/ZnO, N-Li/ZnO, Li-Mg/ZnO, Eu-Er/ZnO, Ni-Cu/ZnO, Al-Li/ZnO, Al-N/ZnO, Cu-V/ZnO, Ag-S/ZnO, Ga-N/ZnO, Al-N/ZnO, Mg-Ga/ZnO, Y-Cd/ZnO, Cd-Al/ZnO, N-In/ZnO and Al-Ga/ZnO [59-61].

In line with the purpose of the present study for enhancing ZnO photocatalytic activity [4, 14, 19, 22], ZnO, Mg/ZnO, La/ZnO and Mg-La/ZnO nanoparticles were synthesized by sol-gel method. To the best of our knowledge, there is no report concerning the co-doping of ZnO with Mg and La. The structural properties of the prepared catalyst were characterized by using X-ray diffraction (XRD), scanning electron microscopy (SEM), transmission electron microscopy (TEM), UV-Vis diffuse reflectance spectroscopy (DRS) and specific surface area and porosity analysis (BET & BJH). The catalytic activity of nanoparticles was investigated with regard to removing Rhodamine B (RhB) under ultraviolet light (UVA).

2 Experimental

2.1 Materials

Zinc acetate di-hydrate ($Zn(CH_3COO)_2.2H_2O$, Merck), Lanthanum nitrate hexa-hydrate ($La(NO_3)_3.6H_2O$, Merck), Magnesium nitrate hexa-hydrate ($Mg(NO_3)_2.6H_2O$, Merck) were used as sources of Zn, La and Mg, respectively. Oxalic acid di-hydrate and ethanol (99.99 %) were also purchased from Merck and used without further purification. Rhodamine B (Merck) was used as model contaminant for the photocatalytic activity experiments. Double distilled water was used in all experiments.

2.2 Synthesis of nanoparticles using sol-gel method

Bimetallic Mg-La/ZnO, monometallic Mg/ZnO and La/ZnO and pure ZnO were prepared by using sol-gel method. For the co-doped ZnO nanoparticles with 5-6 wt.% Mg and 4-5 wt. % La, at first zinc acetate di-hydrate was slowly dissolved in 100 mL ethanol at 60 °C (with thermal controlling) and ongoing stirring for 30 min until homogeneous solution was obtained. Then, appropriate amounts of $Mg(NO_3)_2$ and $La(NO_3)_3$ dissolved in 20 mL ethanol at 60 °C were used which were continuously stirred for 30 min until homogeneous solution was obtained and was added drop by drop to the ethanolic solution of zinc acetate (where temperature was controlled). The oxalic acid, dissolved in ethanol (40 mL) at 60 °C, was added drop by drop to the ethanolic solution. The mixture was stirred for 2 h. The obtained white colloidal semi-gel dried at 90 °C for 12 h in the oven (E24-Sherwood Co). The dried xerogel was calcinated at 400 °C for 2 h in the electric Furnace (ALF-18-iran, Atbin Co). It was powdered by mortar. Doped Mg/ZnO and La/ZnO nanoparticles with 1-6 wt. % and bare ZnO were also prepared by the similar procedure [4, 26, 35, 62, 63].

2.3 Photocatalytic experiments

All experiments regarding photocatalytic degradation were carried out in a batch 100 mL volume quartz photoreactor with a 35 × 2.5 cm dimension which was fixed parallel to UVA light source. During the reaction, oxygen gas was entered from the bottom of the photoreactor. UV-A (Hitachi, F15T8/BL, 15 W, λ_{max} = 370 nm) was the irradiation source. During the photocatalytic reaction,

evaporation could be neglected because the solution temperature did not increase significantly. For photocatalytic RhB degradation through ZnO nanoparticle (bare, doped and co-doped), 50 mL of aqueous RhB solution with fixed weight of catalyst (20 mg) was sonicated for 15 min in ultrasonic bath (Sonica-2200ETH, Italy, 260W, 40 kHz in dimension of 24×14×10 cm). The aqueous RhB solution (10 mg L^{-1}) including the photocatalyst was transferred to the batch quartz photoreactor and bubbled with an oxygen flow to keep the suspension homogeneous (flow rate = 0.5 mL min^{-1}) for 15 min in the darkness. The reaction was initiated by turning on the UVA lamp and 5 mL suspension solution was taken at a certain irradiation time (21 min); then, the nanoparticles were separated by centrifuge (Kokusan H-11n). RhB Concentration was analyzed by UV-Vis spectrophotometer (Biowave-S2100, WPA) at λ_{max} = 554 nm. [4, 19, 26].

2.4 Characterization methods

The crystalline phase and average crystallite size of the synthesized ZnO (bare, doped and co-doped) nanoparticles were characterized using XRD technique via analytical-X'pert Pro-X-ray diffractometer. XRD patterns were recorded using Cu kα irradiation (λ = 0.154 nm) operator at 40 kV and 100 mA in the diffraction range (2θ) between 10 to 80º. The average crystallite size, i.e. D (nm), of the obtained nanoparticles was calculated by Scherrer's equation [64]. The morphology and size of particles were determined by FESEM technique (MIRA3-TE-SCAN Co). FESEM was equipped with an energy dispersive X-ray spectroscopy (EDX) system for analyzing the chemical composition of nanoparticles. The morphology and average size of the nanoparticles were analyzed by TEM (EM10C-100kV-Zeiss, Germany). The optical band gap energy of nanoparticles was obtained by UV-Vis diffuse reflectance spectroscopy (DRS, UV-2550, Shimadzu, Japan). The results of the DRS were converted to the Tauc equation. The optical band gap of nanoparticles can be calculated by Tauc equation (Eq. (1)).

$$\alpha h\nu = A\left(h\nu - Eg\right)^{n} \quad (1)$$

where *Eg* refers to the optical band gap; *h* denotes Planck's constant; *v* refers to the frequency of incident photons; *A* stands for a constant which is called the band tailing parameter; α refers to the absorption coefficient $\left(\alpha = 4\pi k/\lambda\right)$; *k* is the absorption index or absorbance; λ denotes the wavelength in nm) and *n* refers to the index which depends on the type of transition and may have values such as 3/2, 1/2, 2 and 3 corresponding to direct forbidden, direct allowed, indirect allowed and indirect forbidden transitions, respectively.

The band gaps of insulators/semiconductors are categorized into allowed direct and indirect band gaps. Hence, the value of n should be 0.5 in equation [1] for allowed direct band gap. The average band gap can be derived by plotting Tauc's graphs between $\left(\alpha h\nu\right)^2$ versus photon energy $\left(h\nu\right)$ and by extrapolating the linear portion of the spectra to the hν axis [65-70]. The wavelength of absorption edge (λ) was obtained from equation $Eg = 1239.8/\lambda$. [22, 47, 63]. N_2 adsorption and desorption experiments were carried out at 77 K using the BET analyzer (Belsorp Mini) so as to measure specific surface area and pore size distribution based on BET (Brunauer-Emmett-Teller) and BJH (Barret-Joyner-Halender) methods.

3 Results and discussion

3.1 XRD structural studies

The XRD patterns of the nanoparticles ZnO, Mg5%/ZnO, La4%/ZnO, Mg5%-La5%/ZnO and Mg6%-La4%/ZnO are depicted in Fig. 1. All peaks can be well adopted by the hexagonal wurtzite structure crystal according to the standard XRD pattern of ZnO (JCPDS 36-1451) [71]. It appears from the XRD analysis that there are no second impurity peaks corresponding to MgO and La_2O_3. The absence of characteristic reflections related to the Mg and La in the XRD pattern of Mg and/or La/ZnO (doped and co-doped) samples may be attributed to the low loading quantity and appropriate incorporation of La and Mg ions in the ZnO lattice [22]. The 2θ value for (101) diffraction peak (ZnO main peak) in the XRD patterns of ZnO, Mg5%/ZnO, La4%/ZnO, Mg5%-La5%/ZnO and Mg6%-La4%/ZnO are 36.343º, 36.265º, 36.343º, 36.369º and 36.447º, respectively. The ionic radius of Mg ions (0.72 Å) is close to the Zn ions (0.74 Å) but the radius of the La ions (1.03 Å) is larger than that of Zn ions. The shift in the 2θ values and the broadening of the diffraction peaks indicate that the doped ions are successfully incorporated into the ZnO lattice. Due to the notable difference between La and Zn ionic radiuses, it is difficult for La to substitute Zn and La ions are incorporated only in the interstitial sites of the ZnO lattice [72]. Nevertheless, Mg might be able to substitute Zn because of the same ionic radius. The average crystallite size of the nanoparticles was measured from X-ray line broadening of the (101) diffraction peak by means of Debye-Scherrer's equation. The results, given in Table 1, obviously indicate the reduction of ZnO crystalline size by doping La and

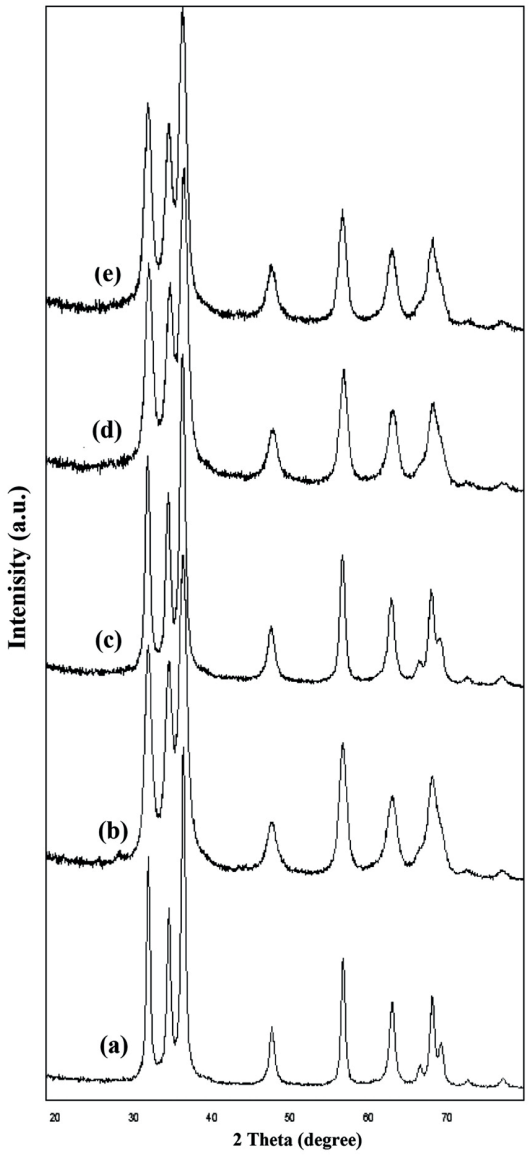

Fig. 1 XRD patterns of (a) ZnO, (b) Mg5%/ZnO, (c) La4%/ZnO, (d) Mg5%-La5%/ZnO, and (e) Mg6%-La4%/ZnO nanoparticles.

Mg. The reduction in crystallite size is mainly attributed to the presence La-O-ZnO and Mg-O-ZnO on the surface of the doped ZnO, which excludes the growth of crystalline grains [26]. In addition, the doping and co-doping of Mg^{2+} and La^{3+} ions lead to oxygen vacancies in the ZnO crystalline structure; consequently, its crystallite size decreases. Due to different La and Mg positions in the ZnO lattice, the impact of Mg doping on the crystallite size was more significant and effective than that of La doping. The micro-strain (ε) can be calculated using in Eq. (2) [29].

$$\varepsilon = \beta \cos\theta / 4 \tag{2}$$

As shown in Table 1, there is a slight change in micro-strain values. That is, the increased micro-strain in nanoparticles changes the diffraction peak broadening which results in a reduction of particle size and a little shift in the XRD peaks. However, it should be pointed out that the line broadening may be due to the size or micro-strain or the interaction between both of them [29]. The cell parameters of prepared samples in Table 1 indicates that the lattice parameter (a) of co-doped nanoparticles are slightly higher than other samples.

3.2 FESEM and EDS studies

FESEM is considered to be a useful technique in studying the structural characterization and morphology of nanoparticles. It has information about the growth mechanism, shape and size of the particles [29]. Fig. 2 (a)-(e) illustrates FESEM images and the surface morphology of bare, doped and co-doped Mg, La/ZnO nanoparticles. It shows that the samples have a uniform spherical-like morphology with a homogenous distribution. Indeed, FESEM images obviously demonstrate that the doping and co-doping of Mg^{2+} and La^{3+} have no impact on the morphology of ZnO nanoparticles; nevertheless, it shows that the size of the grains has decreased, especially in the co-doped sample. In addition to FESEM, EDS analysis was conducted for investigating the chemical composition of nanoparticles. The results of the EDS analysis are depicted in the Fig. 3(a)-(e) and Table 2. EDS spectra of bare ZnO have only two elements, namely Zn and O which indicates that ZnO sample is pure. In addition, doped and co-doped nanoparticles were formed only from Zn, Mg, La and O elements and the purity of the

Table 1 Crystallits size, cell parameters and micro-strain of ZnO, Mg, La doped and co-doped nanoparticles.

Nanoparticle	2θ (deg)	FWHM (β) (rad)	Crystallite size (nm)	Micro-strain (ε)×10^{-3}	Cell parameters	
					a = b (Å)	c (Å)
ZnO	36.343	0.0101	14.28	2.4	3.2200	5.2000
Mg5%/ZnO	36.265	0.0199	7.25	4.7	3.2190	5.1490
La4%/ZnO	36.343	0.0134	10.79	3.2	3.2190	5.1490
Mg5%-La5%/ZnO	36.369	0.0194	7.45	4.6	3.2490	5.2050
Mg6%-La4%/ZnO	36.447	0.0197	7.33	4.7	3.2500	5.2070

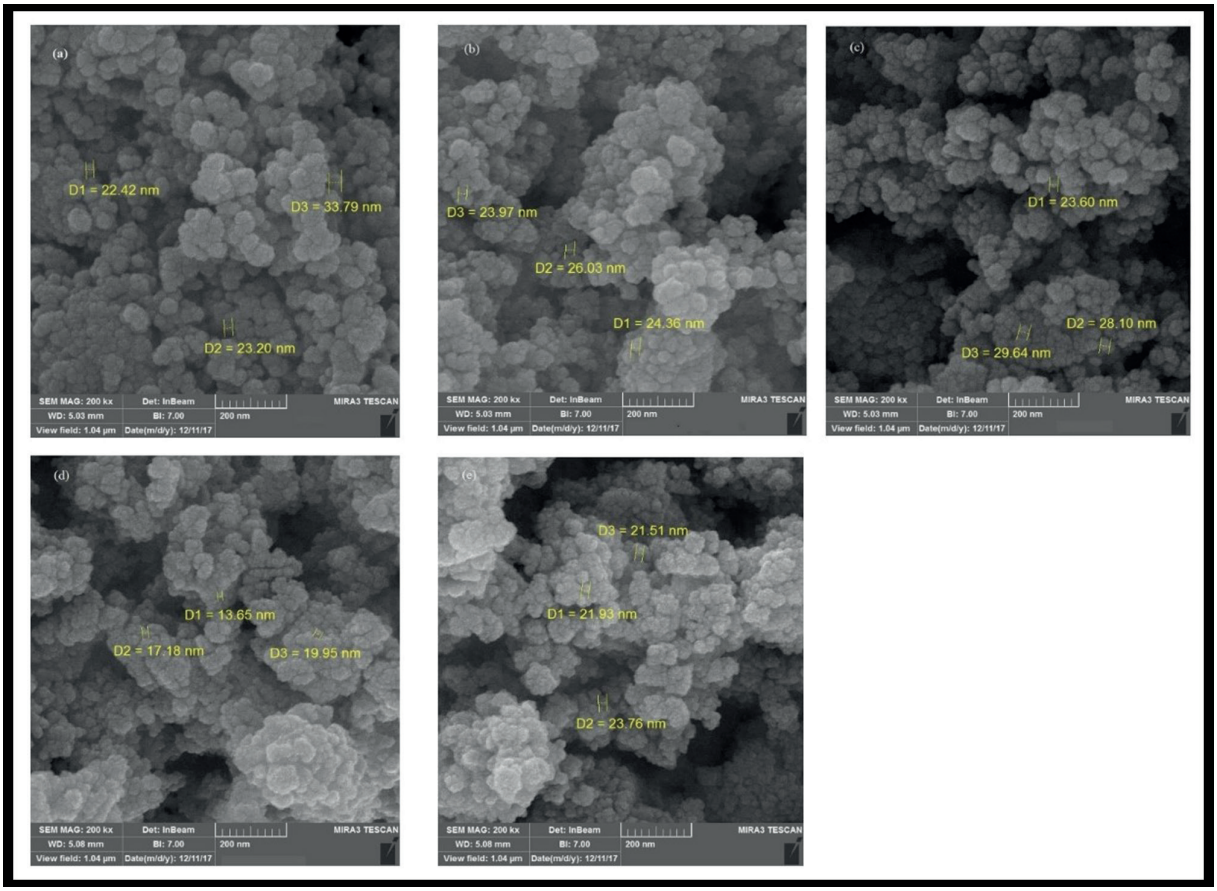

Fig. 2 (a)-(e): FESEM images for (a) ZnO, (b) Mg5%/ZnO, (c) La4%/ZnO, (d) Mg5%-La5%/ZnO and (e) Mg6%-La4%/ZnO

nanoparticles was confirmed. The quantitative analysis of the compositional elements such as Zn, O, Mg and La in the prepared nanoparticles is shown in Table 2. The EDX analysis confirms the presence of Mg and La in ZnO and also indicates good compatibility with the experimental concentration used for the synthesis of nanoparticles.

3.3 TEM images

The shape and size of the particles and their distribution for the prepared nanoparticles are depicted in TEM images (Fig. 4(a)-(e)). TEM images of all samples indicate some agglomeration along with individual particles. According to these images, all prepared photocatalysts have regular distributions and spherical morphology. The size obtained from XRD differs from those of TEM techniques. Whereas the grain size, in TEM, is measured as the distance between visible grain boundaries, the extent of the crystalline region which coherently diffracts X-rays is measured as the grain size in XRD. Consequently, it can be argued that XRD leads to smaller size in comparison with other methods such as TEM and SEM [63]. The particle size distributions based on TEM images for all

Table 2 The quantitative analysis of the compositional elements present in the bare, Mg and La doped and co-doped ZnO nanoparticles.

Samples	Percentage of the element											
	Weight %				Mg/Zn ratio%	La/Zn ratio%	Atomic %				Mg/Zn ratio%	La/Zn ratio%
	Zn	O	Mg	La			Zn	O	Mg	La		
ZnO	79.80	20.20	---	---	---	---	49.15	50.85	---	---	---	---
Mg5%/ZnO	66.09	30.62	3.29	---	4.98	---	34.08	63.93	1.99	---	5.84	---
La4%/ZnO	62.47	35.09	---	2.44	---	3.91	32.36	66.49	---	1.15	---	3.55
Mg5%-La5%/ZnO	58.32	35.68	3.01	2.99	5.16	5.13	38.65	57.31	2.22	1.82	5.74	4.71
Mg6%-La4%/ZnO	56.46	37.67	3.35	2.52	5.93	4.46	36.12	60.05	2.31	1.52	6.39	4.21

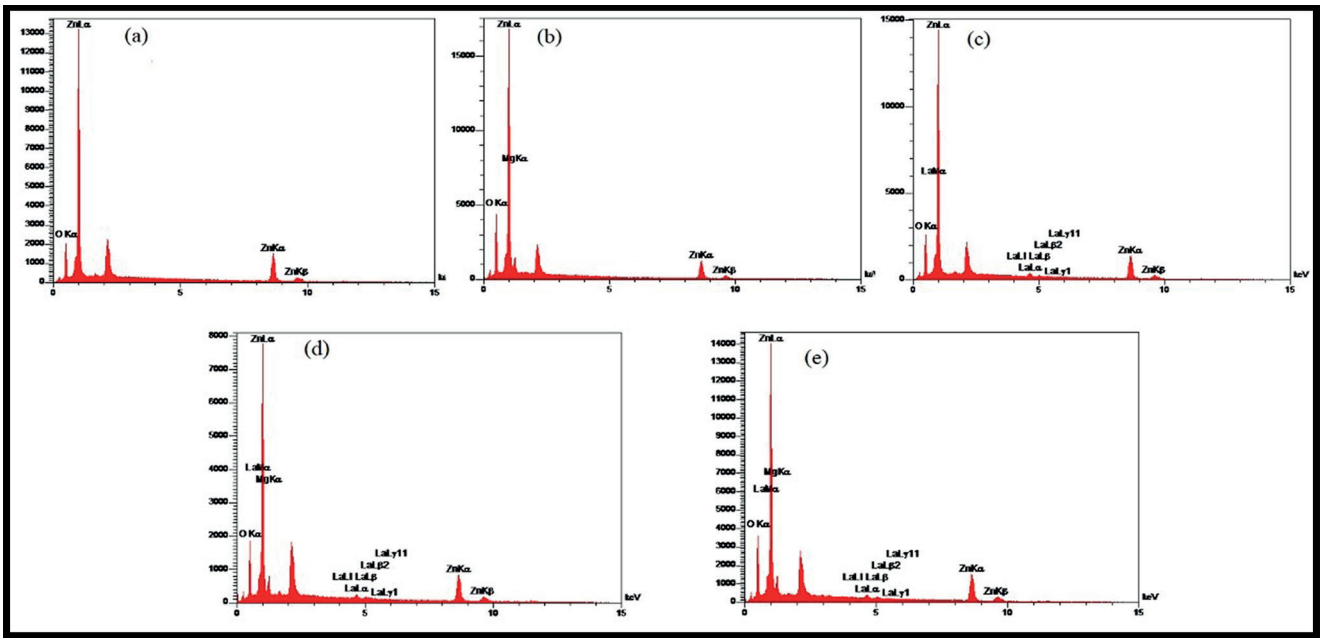

Fig.3 (a)-(e) EDS spectra of (a) bare ZnO, (b) Mg5%/ZnO, (c) La4%/ZnO, (d) Mg5%-La5%/ZnO, and (e) Mg6%-La4%/ZnO

Table 3 Surface area and pore characterization achieved by the BET and BJH methods.

Photocatalyst	BET Surface area ($m^2\ g^{-1}$)	Total Pore Volume ($cm^3\ g^{-1}$)	Mean Pore Diameter (nm)	r_p. Peak (Area) (nm)
ZnO	45.183	0.2728	24.148	14.44
Mg5%/ZnO	72.087	0.5159	28.628	5.35
La4%/ZnO	46.104	0.3130	27.159	12.2
Mg5%-La5%/ZnO	63.621	0.4678	29.409	5.35
Mg6%-La4%/ZnO	54.774	0.3859	28.178	5.35

samples are shown in Fig. 5. The histograms indicate that the average particle size of ZnO, Mg5%/ZnO, La4%/ZnO, Mg5%-La5%/ZnO and Mg6%-La4%/ZnO is about 28.55, 17.62, 23.71, 16.06 and 13.38 nm, respectively. These values were obtained from 569, 540, 618, 490 and 567 particles, respectively. The results reveal that the particle size of nanoparticles is reduced as a result of doping Mg and La into the ZnO lattice.

3.4 BET surface area analysis

Figs. 6(a) and 6(b) depict the N_2 adsorption-desorption isotherms and the pore size distribution for the prepared samples, respectively. According to IUPAC classification, N_2 adsorption-desorption isotherms of the nanoparticles show a type III isotherm which indicates the presence of the mesoporous and macroporous structure [73-76].

The results regarding BET surface area and total pore volume in Table 3 indicate increased surface area and pore volume for the doped and co-doped samples. In the sol-gel technique, crystal growth was suppressed by the addition of La and Mg dopants. Hence, as acknowledged by XRD results, crystallite size decreases; consequently, surface area increases. Moreover, higher surface area values for the doped samples may be attributed to the removal of nitrate from the ZnO lattice during calcination at 400 °C and the thermal decomposition of La and Mg precursors [10]. Thus, increasing the porosity of the surface enhances the surface area [10].

3.5 DRS studies

UV-Vis DRS of nanoparticles are depicted in Fig. 7. The absorption edge of Mg5%/ZnO, La4%/ZnO, and Mg6%-La4%/ZnO are slightly blue shift when compared with bare ZnO nanoparticles. Tauc equation [65, 66] was applied for calculating Eg and absorption edge (Fig. 8). The band gap and absorption edge values for nanoparticles are given in Table 4. ZnO band gap value was enhanced by the doping and co-doping of La and Mg elements. The results reveal that doping with Mg lead to 0.072 eV enhancement in the band gap energy. The resulting 0.039 eV difference

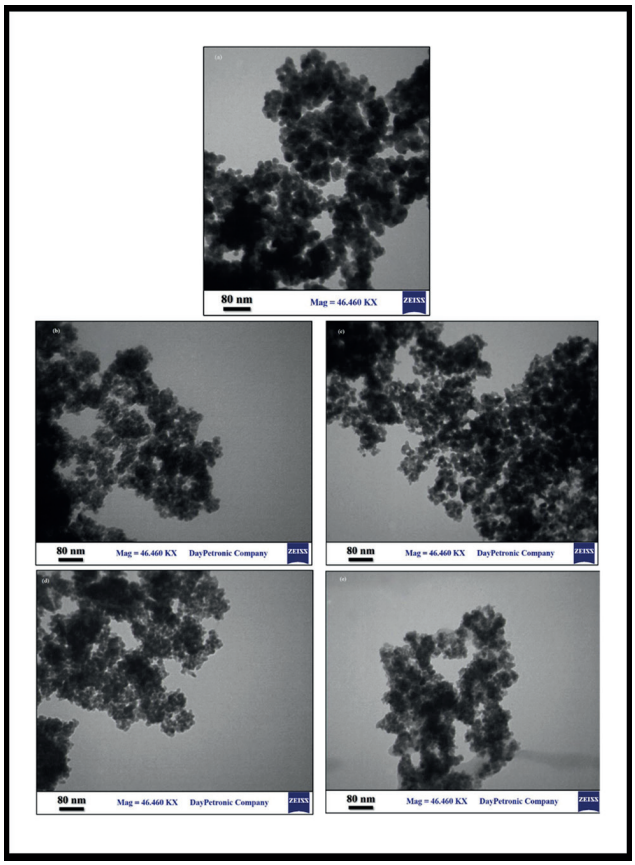

Fig. 4 (a)-(e) TEM images for (a) ZnO, (b) Mg5%/ZnO, (c) La4%/ZnO, (d) Mg5%-La5%/ZnO, and (e) Mg6%-La4%/ZnO nanoparticles.

in bang gap by La doping may be attributed to the decrease in the particle size. According to XRD and TEM results, there is a noticeable decrease in the particle size of doped and co-doped nanoparticles. As the particle size decreases, the energy levels discrete and, eventually, the band gap energy increases. The increasing in the band gap energy and blue shift in the absorption edge by doping of La and Mg ions may be attributed to the Burstein-Moss effect. This effect is caused by the transition energy in degenerate nanoparticles according to the partial field conduction band [36, 77]. Furthermore, shift to lower wavelength or higher energy, blue shift, is due to decreasing the grain size [63]. The blue shift can be attributed to the quantum size effect in nanoparticles [29, 77], distortion of host lattice and defect generation [29]. Gopalakrishnan and Muthukumaran [29], found that increasing ZnO band gap with Ni doping may be due to sp-d spin exchange interaction between band electrons and localized spin of the transition metal ions. Osei-Bonsu Oppong et al. [78] argued that, since d-d transition is superior to sp-d transition, La doping in ZnO lattice enhances band gap energy. When the band gap in the nanoparticles enlarges, the separation of the photo-induced electron-hole pairs occurs better [22].

Table 4 Band gap energy and absorption edge for the prepared nanoparticles.

Photocatalyst	Eg (eV)	λ (nm)
ZnO	3.111	398.52
Mg5%/ZnO	3.183	389.51
La4%/ZnO	3.150	393.59
Mg6%-La4%/ZnO	3.175	390.49

3.6 Photocatalytic Activity

The main purpose of the study is to examine the photocatalytic activity of the prepared nanoparticles. The photocatalytic activity of the bare, doped and co-doped samples in the removal of RhB under UVA irradiation has been shown in Table 5. Blank tests results indicated that the removal percent of RhB by UVA alone (photolysis) and adsorption on nanoparticles was negligible.

The results, given in Table 5, obviously reveal that, as Mg doping increases up to 5 wt. %, RhB removal percent increases significantly. The photocatalytic activity of semiconductor nanoparticles is proportional with their band gap energy. That is, higher band gap energy corresponds with stronger electron-hole pairs which, consequently, lead to higher photocatalytic activity [4]. According to DRS results, Mg-doped ZnO has a larger band gap than bare ZnO, which may account for the higher photocatalytic activity of doped samples. Moreover, the increased Mg dopant leads to more crystal deficiency. Crystal deficiency retards recombination of the electron-hole pair and leads to improved photocatalytic activity [4]. Xue et al. [79], reported that most Mg ions were substituted in the Zn sites of ZnO, which resulted in an increase not only in ZnO band gap, but also in the quality of ZnO crystalline.

Prabu and Johnson [80] argued that the formation of intrinsic defects in the ZnS lattice is due to the incorporation of Mg^{2+}.

However, Mg content values greater than 5 wt. % decreased the photocatalytic activity of ZnO nanoparticles. Such a reduction is attributed to the aggregation of Mg dopant and the reduction of homogeneous distribution of dopant in the ZnO lattice [81]. As shown in Table 5, it is observed that photocatalytic activity significantly enhanced along with La doping up to 4 wt. %. La^{3+} due to existence of a partially filled orbital effectively scavenges photoinduced electrons and produces unstable La^{2+} [82].

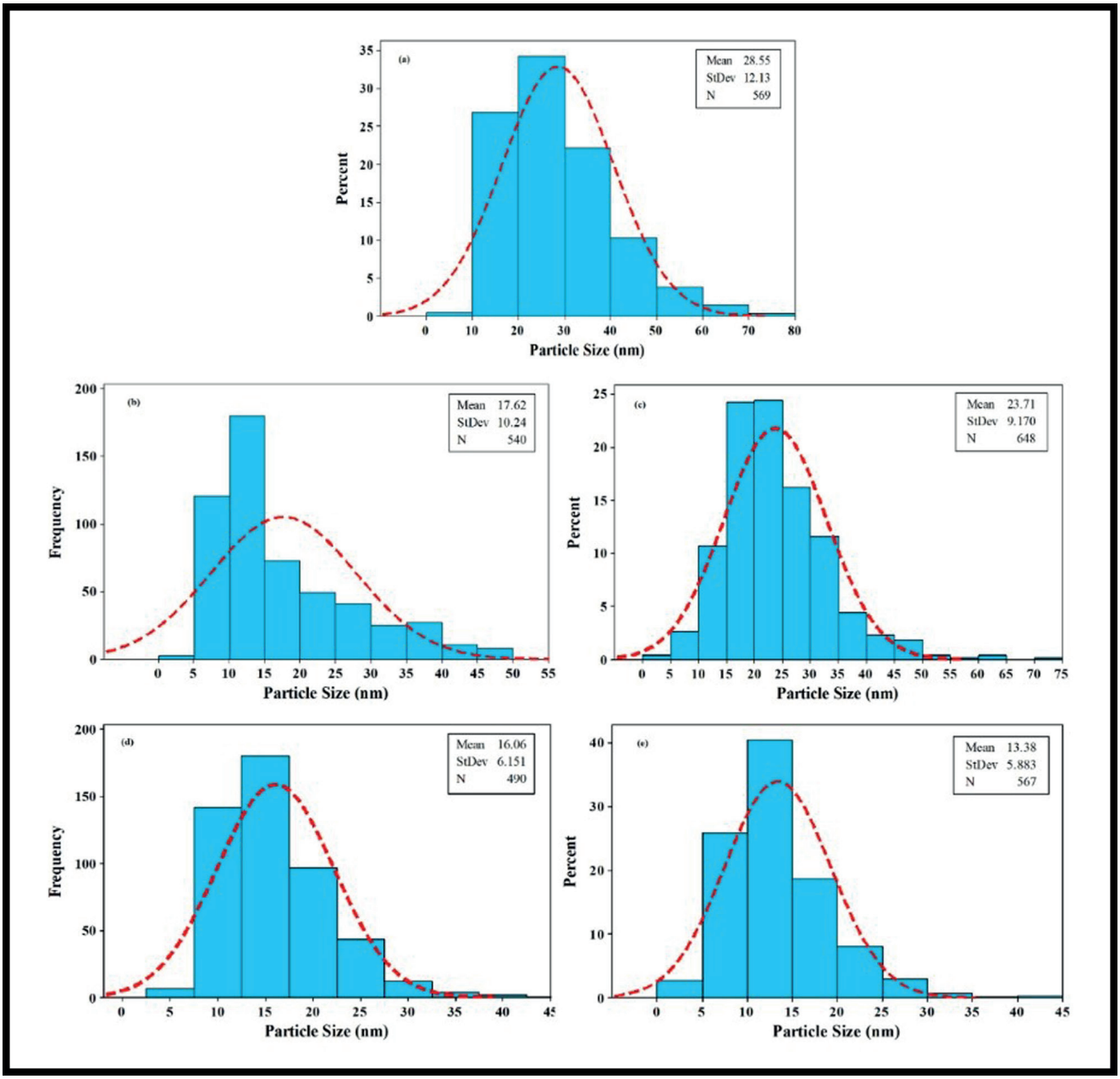

Fig. 5 Histograms of particles size distribution of (a) ZnO, (b) Mg5%/ZnO, (c) La4%/ZnO, (d) Mg5%-La5%/ZnO, and (e) Mg6%-La4%/ZnO nanoparticles.

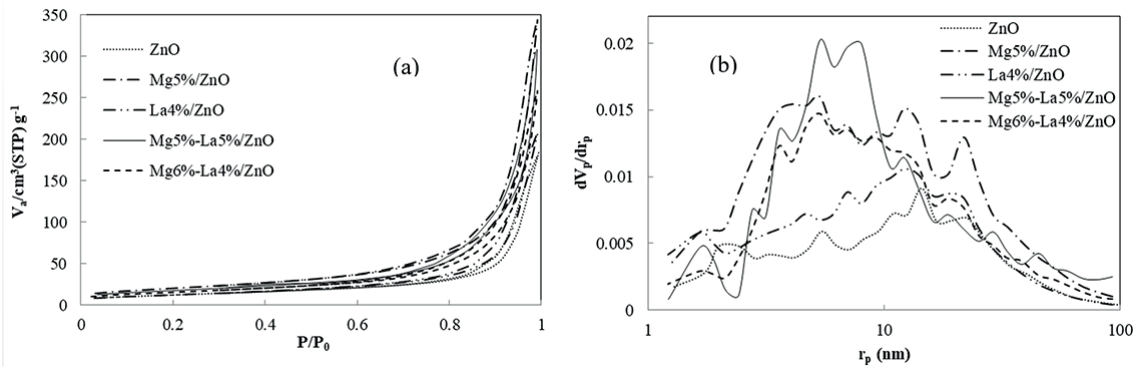

Fig. 6 Adsorption-desorption isotherm (a) and BJH diagrams (b) for prepared nanoparticles.

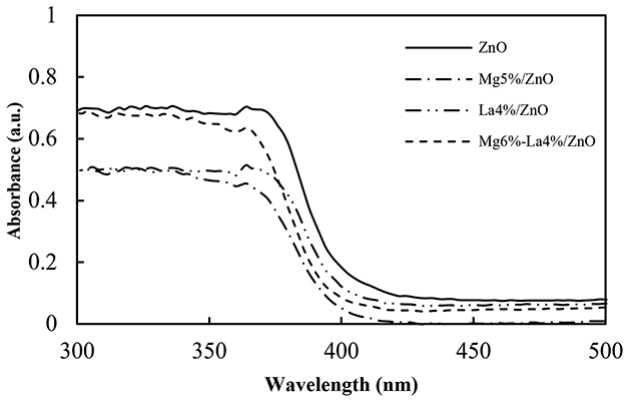

Fig. 7 The DRS-UV-Vis spectra for the prepared nanoparticles.

Table 5 The photocatalytic removal percent of RhB in the presence of various catalysts.

Photocatalyst	Metal loading (wt. %)		Removal percent
	Mg	La	
bare ZnO	0	0	55.40
Mg/ZnO	1	0	58.83
Mg/ZnO	2	0	60.10
Mg/ZnO	3	0	63.07
Mg/ZnO	4	0	65.07
Mg/ZnO	5	0	83.18
Mg/ZnO	6	0	81.96
La/ZnO	0	1	77.77
La/ZnO	0	2	81.96
La/ZnO	0	3	83.87
La/ZnO	0	4	85.18
La/ZnO	0	5	75.38
La/ZnO	0	6	71.89
Mg-La/ZnO	5	5	91.18
Mg-La/ZnO	6	4	89.18

In air-equilibrated system, electron discharges into the dissolved oxygen to form the $O_2^{-\circ}$ and $^{\circ}OH$ as follows:

$$O_2 + e_{CB}^- \rightarrow O_2^{-\circ}, \tag{3}$$

$$O_2 + H^+ + e_{CB}^- \rightarrow HO_2^{\circ}, \tag{4}$$

$$O_2 + 2H^+ + 2e_{CB}^- \rightarrow H_2O_2. \tag{5}$$

In addition, HO_2° and $O_2^{-\circ}$ react with each other to produce H_2O_2 according to Eq. (6):

$$HO_2^{\circ} + O_2^{-\circ} + H^+ \rightarrow H_2O_2 + O_2. \tag{6}$$

The produced H_2O_2 in Eqs. (5), (6) reacts with photoinduced electrons which lead to the production of hydroxyl radicals (Eq. (7)). Hydroxyl radicals can effectively participate non-selectively in the degradation of target molecules.

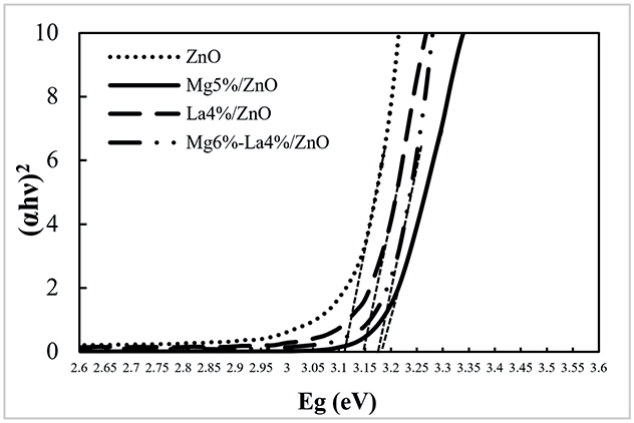

Fig. 8 Tauc plot and band gap energy estimation for the prepared nanoparticles.

$$H_2O_2 + H^+ + e_{CB}^- \rightarrow H_2O + {}^{\circ}OH. \tag{7}$$

Jia et al. [77], found that La doping produces surface defects and a space charge layer in the surface of La-doped ZnO samples, which hinders recombination of photoinduced electron - hole pairs. However, when the La amount exceeds 4 wt. %, the photocatalytic activity is notably reduced which is attributed to the aggregation of La_2O_3 and to the negative impact of surface charge layer [77]. Covering ZnO surface from light absorption at higher doping values is another reason for decreasing photocatalytic activity [65]. Tayade et al. [83], maintained that ions with an ionic radius higher than the host element occupy the interstitial positions; however, ions with an ionic radius near the host element occupy the substitutional positions. Also, they found that the occupation of interstitial positions is more effective in the photocatalytic activity than the occupation of the substitutional positions. In the present study, La^{3+} ions have an ionic radius which is greater than that of the host element (Zn^{2+}); nevertheless, Mg^{2+} ions have an ionic radius which is close to that of Zn^{2+} ions. Therefore, La^{3+} and Mg^{2+} ions are expected to occupy interstitial and substitutional positions in ZnO lattice, respectively. That is why La-doped ZnO has higher photocatalytic activity up to 4 % (La optimum percent) than Mg-doped ZnO. According to the results given in Table 5, co-doped Mg-La/ZnO has higher photocatalytic activity than mono-doped and bare ZnO. The higher photocatalytic activity of the co-doped Mg-La/ZnO may be due to different sites of La^{3+} and Mg^{2+} ions in ZnO lattice so that La^{3+} in the interstitial positions and Mg^{2+} in the substitutional positions. On the other hand, Mg doping increases band gap and ZnO surface area. Consequently, the increased band gap has a critical impact on photocatalytic activity. Firstly, a catalyst with a wide band gap absorbs less light. Due to the

emission wavelength of the lamp (365 nm), the reduced light absorption is not important in this study. According to Table 4, all catalysts can absorb wavelengths less than 390 nm. Secondly, a wider band gap corresponds with better separation and also with stronger photoinduced electron-hole pairs. Thus, it can be argued that a wider band gap improves photocatalytic activity. Increasing the specific surface area with Mg doping is another important factor for higher photocatalytic activity. A higher specific surface area enhances RhB adsorption and active sites, which, consequently, have notable positive impacts on photocatalytic activity. In addition, La with partially filled orbital and a space charge layer in the surface scavenges photoinduced electrons and enhances photocatalytic activity.

4 Conclusion

In this study, Mg and La doped and co-doped ZnO nanoparticles were successfully prepared by the sol-gel method. The XRD results of nanoparticles did not show the presence of separate metal oxide diffraction peaks for Mg and La phases due to the proper incorporation of doped ions. The FESEM, EDX and TEM results confirmed that all the prepared nanoparticles had a uniform spherical-like morphology with a homogenous distribution; however, the grain size of the nanoparticles decreased due to the doping and co-doping processes. The DRS results indicated a significant increase in Eg for Mg and La doped and co-doped ZnO nanoparticles. N_2 adsorption-desorption results indicated an increase in BET surface area and pore volume for doped and co-doped ZnO nanoparticles. Mg5%-La5%/ZnO had the highest capability for photocatalytic RhB removal in comparison with mono-doped and bare ZnO.

Acknowledgments

The authors would like to gratefully acknowledge the supports of Islamic Azad University, North Tehran Branch and Ardabil Branch.

References

[1] Baruah, S., Pal, S. K., Dutta, J. "Nanostructured Zinc Oxide for Water Treatment", Nanoscience and Nanotechnology-Asia, 2(2), pp. 90–102, 2012. https://doi.org/10.2174/2210681211202020090

[2] Han, F., Kambala, V. S. R., Srinivasan, M., Rajarathnam, D., Naidu, R. "Tailored Titanium Dioxide Photocatalysts for the Degradation of Organic Dyes in Wastewater Treatment: A Review", Applied Catalysis A: General, 359(1-2), pp. 25–40, 2009. https://doi.org/10.1016/j.apcata.2009.02.043

[3] Alfano, O. M., Bahnemann, D., Cassano, A. E., Dillert, R., Goslich, R. "Photocatalysis in Water Environments Using Artificial and Solar light", Catalysis Today, 58(2-3), pp. 199–230, 2000. https://doi.org/10.1016/S0920-5861(00)00252-2

[4] Zarei, N., Behnajady, M. A. "Synthesis, Characterization, and Photocatalytic Activity of Sol-gel Prepared Mg/ZnO Nanoparticles", Desalination and Water Treatment, 57(36), pp. 1–7, 2015. https://doi.org/10.1080/19443994.2015.1083479

[5] Khataee, A., Karimi, A., Arefi-Oskoui, S., Darvish, R., Hanifehpour, Y., Soltani, B., Joo, S. W. "Sonochemical Synthesis of Pr-doped ZnO Nanoparticles for Sonocatalytic Degradation of Acid Red 17", Ultrasonics Sonochemistry, 22, pp. 371–381, 2015. https://doi.org/10.1016/j.ultsonch.2014.05.023

[6] Modirshahla, N., Behnajady, M. A., Mohammadi-Aghdam, S. "Investigation of the effect of different electrodes and their connections on the removal efficiency of 4-nitrophenol from aqueous solution by electrocoagulation", Journal of Hazardous Materials, 154, pp. 778–786, 2008. https://doi.org/10.1016/j.jhazmat.2007.10.120

[7] Ahmad, M., Ahmed, E., Hong, Z. L., Ahmed, W., Elhissi, A., Khalid, N. R. "Photocatalytic, Sonocatalytic and Sonophotocatalytic Degradation of Rhodamine B Using ZnO/CNTs Composites Photocatalysts", Ultrasonics Sonochemistry, 21(2), pp. 761–773, 2014. https://doi.org/10.1016/j.ultsonch.2013.08.014

[8] Xiao, J., Xie, Y., Cao, H., Nawaz, F., Zhang, S., Wang, Y. "Disparate Roles of Doped Metal Ions in Promoting Surface Oxidation of TiO_2 Photocatalysis", Journal of Photochemistry and Photobiology A: Chemistry, 315, pp. 59–66, 2016. https://doi.org/10.1016/j.jphotochem.2015.09.013

[9] Chatterjee, D., Dasgupta, S. "Visible Light Induced Photocatalytic Degradation of Organic Pollutants", Journal of Photochemistry and Photobiology C: Photochemistry Reviews, 6(2-3), pp. 186–205, 2005. https://doi.org/10.1016/j.jphotochemrev.2005.09.001

[10] Segne, T. A., Tirukkovalluri, S. R., Challapalli, S. "Studies on Characterization and Photocatalytic Activities of Visible Light Sensitive TiO_2 Nanocatalysts co-doped with Magnesium and Copper", International Research Journal of Pure and Applied Chemistry, 1, pp. 84–103, 2011. https://doi.org/10.9734/IRJPAC/2011/453

[11] Eren, Z., Ince, N. H. "Sonolytic and Sonocatalytic Degradation of Azo Dyes by Low and High Frequency Ultrasound", Journal of Hazardous Materials, 177(1-3), pp. 1019–1024, 2010. https://doi.org/10.1016/j.jhazmat.2010.01.021

[12] Bokhale, N. B., Bomble, S. D., Dalbhanjan, R. R., Mahale, D. D., Hinge, S. P., Banerjee, B. S., Mohod, A. V., Gogate, P. R. "Sonocatalytic and Sonophotocatalytic Degradation of Rhodamine 6G Containing Wastewaters", Ultrasonics Sonochemistry, 21(5), pp. 1797–1804, 2014. https://doi.org/10.1016/j.ultsonch.2014.03.022

[13] Rauf, M.A., Meetani, M.A., Hisaindee, S. "An Overview on the Photocatalytic Degradation of Azo Dyes in the Presence of TiO_2 Doped with Selective Transition Metals", Desalination, 276(1-3), pp. 13–27, 2011. https://doi.org/10.1016/j.desal.2011.03.071

[14] Behnajady, M. A., Tohidi, Y. "Synthesis, Characterization and Photocatalytic Activity of Mg-impregnated ZnO-SnO_2 Coupled Nanoparticles", Photochemistry and Photobiology, 90(1), pp. 51–56, 2014.
https://doi.org/10.1111/php.12164

[15] Choina, J., Dolat, D., Kusiak, E., Janus, M., Morawski, A. W. "TiO_2 Modified by Ammonia as a Long Lifetime Photocatalyst for Dyes Decomposition", Polish Journal of Chemical Technology, 11(4), pp. 1–6, 2009.
https://doi.org/10.2478/v10026-009-0035-9

[16] Lodha, S., Jain, A., Punjabi, P. B. "A Novel Route for Waste Water Treatment: Photocatalytic Degradation of Rhodamine B", Arabian Journal of Chemistry, 4(4), pp. 383–387, 2011.
https://doi.org/10.1016/j.arabjc.2010.07.008

[17] Abdollahi, Y., Zakaria, A., Abbasiyannejad, M., Masoumi, H. R. F., Moghaddam, M. G., Matori, K. A., Jahangirian, H., Keshavarzi, A. "Artificial Neural Network Modeling of p-Cresol Photodegradation", Chemistry Central Journal, 96(7), pp. 1–7, 2013.
https://doi.org/10.1186/1752-153X-7-96

[18] Zouaghi, R., David, B., Suptil, J., Djebbar, K., Boutiti, A., Guittonneau, S. "Sonochemical and Sonocatalytic Degradation of Monolinuron in Water", Ultrasonics Sonochemistry, 18(5), pp. 1107–1112, 2011.
https://doi.org/10.1016/j.ultsonch.2011.03.008

[19] Behnajady, M. A., Modirshahla, N., Shokri, M., Zeininezhad, A., Zamani, H. A. "Enhancement Photocatalytic Activity of ZnO Nanoparticles by Silver Doping with Optimization of Photodeposition Method Parameters", Journal of Environmental Science and Health, Part A, 44(7), pp. 666–672, 2009.
https://doi.org/10.1080/10934520902847752

[20] Ghaly, M. Y., Ali, M. E. M., Osterlund, L., Khattab, I. A., Badawy, M. I., Farah, J. Y., Zaher, F. M., Al-Maghrabi, M. N. εZnO/spiral-shaped Glass for Solar Photocatalytic Oxidation of Reactive Red120", Arabian Journal of Chemistry, 10(2), pp. S3501–S3507, 2017.
https://doi.org/10.1016/j.arabjc.2014.02.015

[21] Behnajady, M. A., Eskandarloo, H. "Silver and Copper Co-impregnated onto TiO_2-P25 Nanoparticles and its Photocatalytic Activity", Chemical Engineering Journal, 228(15), pp. 1207–1213, 2013.
https://doi.org/10.1016/j.cej.2013.04.110

[22] Eskandarloo, H., Badiei, A., Behnajady, M. A., Ziarani, G. M. "Ultrasonic-assisted Degradation of Phenazopyridine with a Combination of Sm-doped ZnO Nanoparticles and Inorganic Oxidants", Ultrasonics Sonochemistry, 28, pp. 169–177, 2016.
https://doi.org/10.1016/j.ultsonch.2015.07.012

[23] Lee, S. D., Nam, S-H., Kim, M-H., Boo, J-H. "Synthesis and Photocatalytic Property of ZnO Nanoparticles Prepared by Spray-pyrolysis Method", Physics Procedia, 32, pp. 320–326, 2012.
https://doi.org/10.1016/j.phpro.2012.03.563

[24] Al-Owais, A. A. "Synthesis and Magnetic Properties of Hexagonally Packed ZnO Nanorods", Arabian Journal of Chemistry, 6(2), pp. 229–234, 2013.
https://doi.org/10.1016/j.arabjc.2011.11.001

[25] Cuevas, A. G., Balangcod, K., Balangcod, T., Jasmin, A. "Surface Morphology, Optical Properties and Antibacterial Activity of Zinc Oxide Films Synthesized via Spray Pyrolysis", Procedia Engineering, 68, pp. 537–543, 2013.
https://doi.org/10.1016/j.proeng.2013.12.218

[26] Anandan, S., Vinu, A., Mori, T., Gokulakrishnan, N., Srinivasu, P., Murugesan, V., Ariga, K. "Photocatalytic Degradation of 2,4,6-Trichlorophenol Using Lanthanum Doped ZnO in Aqueous Suspension", Catalysis Communications, 8(9), pp. 1377–1382, 2007.
https://doi.org/10.1016/j.catcom.2006.12.001

[27] Kaneva, N. V., Dushkin, C. D. "Preparation of Nanocrystalline Thin Films of ZnO by Sol-gel Dip Coating", Bulgarian Chemical Communications, 43(2), pp. 259–263, 2011. [online] Available at: http://www.bgcryst.com/symp10/proceeding/12_Kaneva_259-263.pdf [Accessed: 06 August 2018]

[28] Sivakumar, K., Kumar, V. S., Muthukumarasamy, N., Thambidurai, M., Senthil, T. S. "Influence of pH on ZnO Nanocrystalline Thin Films Prepared by Sol-gel Dip Coating Method", Bulletin of Materials Science, 35(3), pp. 327–331, 2012.
https://doi.org/10.1007/s12034-012-0305-7

[29] Gopalakrishnan, R., Muthukumaran, S. "Nanostructure, Optical and Photoluminescence Properties of $Zn_{1-X}Ni_XO$ Nanoclusters by Co-Precipitation Method", Journal of Materials Science: Materials in Electronics, 24(4), pp. 1069–1080, 2013.
https://doi.org/10.1007/S10854-012-0882-7

[30] Chauhan, R., Kumar, A., Chaudhary, R. P. "Synthesis and Characterization of Silver Doped ZnO Nanoparticles", Archives of Applied Science Research, 2(5), pp. 378–385, 2010. [online] Available at: https://www.scholarsresearchlibrary.com/articles/synthesis-and-characterization-of-silver-doped-zno-nanoparticles.pdf [Accessed: 07 August 2018]

[31] Young, S. J., Ji, L. W., Chang, S. J., Liang, S. H., Lam, K. T., Fang, T. H., Chen, K. J., Du, X. L., Xue, Q. K. "ZnO-based MIS Photodetectors", Sensors and Actuators A:Physical, 141(1), pp. 225–229, 2008.
https://doi.org/10.1016/j.sna.2007.06.003

[32] Ni, G., Chen, Y., Liu, Y., Liu, H., Zhang, Z. "Fabrication of ZnO Nanoparticles for Photocatalytic Reduction of CO_2", MATEC Web of Conferences, 67, ID 02009, 2016.
https://doi.org/10.1051/matecconf/20166702009

[33] Han, J., Liu, Y., Singhal, N., Wang, L., Gao, W. "Comparative Photocatalytic Degradation of Estrone in Water by ZnO and TiO_2 under Artificial UVA and Solar Irradiation", Chemical Engineering Journal, 213(1), pp. 150–162, 2012.
https://doi.org/10.1016/j.cej.2012.09.066

[34] Eskandarloo, H., Badiei, A., Behnajady, M. A., Ziarani, G. M. "Ultrasonic-assisted Sol-gel Synthesis of Samarium, Cerium Co-doped TiO_2 Nanoparticles with Enhanced Sonocatalytic Efficiency", Ultrasonics Sonochemistry, 26, pp. 281–292, 2015.
https://doi.org/10.1016/j.ultsonch.2015.02.001

[35] Georgekutty, R., Seery, M. K., Pillai, S. C. "A Highly Efficient Ag-ZnO Photocatalyst: Synthesis, Properties, and Mechanism", The Journal of Physical Chemistry C, 112(35), pp. 13563–13570, 2008.
https://doi.org/10.1021/jp802729a

[36] Bloh, J. Z., Dillert, R., Bahnemann, D. W. "Transition Metal-Modified Zinc Oxides for UV and Visible Light Photocatalysis", Environmental Science and Pollution Research, 19(9), pp. 3688–3695, 2012. https://doi.org/10.1007/s11356-012-0932-y

[37] Safaei-Ghomi, J., Ghasemzadeh, M. A. "Zinc Oxide Nanoparticle Promoted Highly Efficient One Pot Three-component Synthesis of 2,3-Disubstituted Benzofurans", Arabian Journal of Chemistry, 10(2), pp. S1774–S1780, 2017. https://doi.org/10.1016/j.arabjc.2013.06.030

[38] Rajendran, S., Mansoob Khan, M., Gracia, F., Qin, J., Gupta. V. K., Arumainathan, S. "Ce^{3+} ion-induced visible-light photocatalytic degradation and electrochemical activity of ZnO/CeO_2 nanocomposite", Scientific Reports, 6(1), pp. 1–11, 2016. https://doi.org/10.1038/srep31641

[39] Saravanan, R., Mansoob Khan, M., Gupta, V.K., Mosquera, E., Gracia, F., Narayanan, V., Stephen, A. "ZnO/Ag/Mn_2O_3 nanocomposite for visible light-induced industrial textile effluent degradation, uric acid and ascorbic acid sensing and antimicrobial activity", RSC Advances, 5(44) pp. 34645–34651, 2015. https://doi.org/10.1039/C5RA02557E

[40] Saravanan, R., Karthikeyan, N., Gupta, V.K., Thirumal, E., Thangadurai, P., Narayanan, V., Stephen, A. "ZnO/Ag nanocomposite: An efficient catalyst for degradation studies of textile effluents under visible light", Materials Science & Engineering: C, Materials for Biological Applications, 33(4), pp. 2235–2244, 2013. https://doi.org/10.1016/j.msec.2013.01.046

[41] Saravanan, R., Gupta, V. K., Prakash, T., Narayanan, V., Stephen, A. "Synthesis, Characterization and Photocatalytic Activity of Novel Hg doped ZnO Nanorods prepared by Thermal Decomposition Method", Journal of Molecular Liquids, 178, pp. 88–93, 2013. https://doi.org/10.1016/j.molliq.2012.11.012

[42] Saravanan, R., Gracia, F., Mansoob Khan, M., Poornima, Gupta, V. K., Narayanan, V., Stephen., A. "ZnO/CdO nanocomposites for textile effluent degradation and electrochemical detection", Journal of Molecular Liquids, 209, pp. 374–380, 2015. https://doi.org/10.1016/j.molliq.2015.05.040

[43] Saravanan, R., Gupta, V.K., Narayanan, V., Stephen, A. "Visible light degradation of textile effluent using novel catalyst ZnO/γ-Mn_2O_3", Journal of the Taiwan Institute of Chemical Engineers, 45 (4), pp. 1910–1917, 2014. https://doi.org/10.1016/j.jtice.2013.12.021

[44] Saravanan, R., Gupta, V. K., Mosquera, E., Gracia, F. "Preparation and characterization of V_2O_5/ZnO nanocomposite system for photocatalytic application", Journal of Molecular Liquids, 198, pp. 409–412, 2014. https://doi.org/10.1016/j.molliq.2014.07.030

[45] Saravanan, R., Karthikeyan, S., Gupta, V.K., Sekaran, G., Narayanan, V., Stephen, A. "Enhanced photocatalytic activity of ZnO/CuO nanocomposite for the degradation of textile dye on visible light illumination", Materials Science & Engineering: C, Materials for Biological Applications, 33(1), pp. 91–98, 2013. https://doi.org/10.1016/j.msec.2012.08.011

[46] Thaweesaeng, N., Supankit, S., Techidheera, W., Pecharapa, W. "Structure Properties of As-synthesized Cu-doped ZnO Nanopowder Synthesized by Co-Precipitation Method", Energy Procedia, 34, pp. 682–688, 2013. https://doi.org/10.1016/j.egypro.2013.06.800

[47] Sankara, R. B., Venkatramana, R. S., Koteeswara, R. N., Pramoda, K. J. "Synthesis, Structural, Optical Properties and Antibacterial Activity of co-doped (Ag, Co) ZnO Nanoparticles", Research Journal of Material Sciences, 1(1), pp.11-20, 2013. [online] Available at: http://www.isca.in/MATERIAL_SCI/Archive/v1/i1/3.ISCA-RJMatS-2013-003.pdf [Accessed: 07 August 2018]

[48] Anand, M., Shim, H-S., Kim, Y. S., Kim, W. B. "Structural and Optical Properties of Co- and Ti-ZnO Composite Nanofibers Prepared by Using an Electrospinning Method", Journal of the Korean Physical Society, 53, pp. 2423–2426, 2008. https://doi.org/10.3938/jkps.53.2423

[49] Cao, H. T., Pei, Z. L., Gong, J., Sun, C., Huang, R. F., Wen, L. S. "Transparent Conductive Al and Mn Doped ZnO Thin Films Prepared by DC Reactive Magnetron Sputtering", Surface and Coatings Technology, 184(1), pp. 84–92, 2004. https://doi.org/10.1016/j.surfcoat.2003.09.046

[50] Chongsri, K., Bangbai, C., Techitdheera, W., Pecharapa, W. "Characterization and Photoresponse Properties of Sn-doped ZnO Thin Films", Energy Procedia, 34, pp. 721–727, 2013. https://doi.org/10.1016/j.egypro.2013.06.805

[51] Dakhel, A. A., El-Hilo, M. "Ferromagnetic Nanocrystalline Gd-doped ZnO Powder Synthesized by Coprecipitation", Journal of Applied Physics, 107(12), ID: 123905-6, 2010. https://doi.org/10.1063/1.3448026

[52] Ali, A. M., Muhammad, A., Shafeeq, A., Asghar, H. M. A., Hussain, S. N., Sattar, H. "Doped Metal Oxide (ZnO) and Photocatalysis: A Review", Journal of Pakistan Institute of Chemical Engineers, 40(1), pp. 11–19, 2012. [online] Available at: http://piche.org.pk/journal/index.php?journal=jpiche&page=article&op=view&path%5B%5D=52 [Accessed: 07 August 2018]

[53] Benelmadjat, H., Boudine, B., Keffous, A., Gabouze, N. "Photoresponse and H_2 Gas Sensing Properties of Highly Oriented Al and Al/Sb Doped ZnO Thin Films", Progress in Natural Science: Materials International, 23(6), pp. 519–523, 2013. https://doi.org/10.1016/j.pnsc.2013.11.001

[54] Zhang, W., Zhao, J., Liu, Z., Liu, Zh. "Structural, Optical and Magnetic Properties of $Zn_{1-X}Fe_XO$ Powders by Sol-gel Method", Applied Surface Science, 284, pp. 49–52, 2013. https://doi.org/10.1016/j.apsusc.2013.06.163

[55] Pillai, S. C., Kelly, J. M., Ramesh, R., Mccormach, D. E. "Advances in the Synthesis of ZnO Nanomaterials for Varistor Devices", Journal of Materials Chemistry C, 1(20), pp. 3268–3281, 2013. https://doi.org/10.1039/c3tc00575e

[56] Behnajady, M. A., Alizade, B., Modirshahla, N. "Synthesis of Mg-Doped TiO_2 Nanoparticles under Different Conditions and its Photocatalytic Activity", Photochemistry and Photobiology, 87(6), pp. 1308–1314, 2011. https://doi.org/10.1111/j.1751-1097.2011.01002.x

[57] Feng, H., Yu, L. E., Zhang, M. H., Zakaria, M. H. "Ultrasonic Synthesis and Photocatalytic Performance of Metal-Ions Doped TiO_2 Catalysts under Solar Light Irradiation", Materials Research Bulletin, 48(2), pp. 672–681, 2013. https://doi.org/10.1016/j.materresbull.2012.11.027

[58] Wang, H., Baek, S., Lee, J., Lim, S. "High Photocatalytic Activity of Silver-Loaded ZnO-SnO_2 Coupled Catalyst", The Chemical Engineering Journal, 146(3), pp. 355–361, 2009. https://doi.org/10.1016/j.cej.2008.06.016

[59] Lee, M.-I., Huang, M.-C., Legrand, D., Lerondel, G., Lin, J.-C. "Structure and characterization of Sn, Al co-doped zinc oxide thin films prepared by sol–gel dip-coating process", Thin Solid Films, 570B, pp. 516–526, 2014.
https://doi.org/10.1016/j.tsf.2014.04.051

[60] Tian, X., Pan, Z., Zhang, H., Fan, H., Zeng, X., Xiao, C., Hu, G., Wei, Z. "Growth and characterization of the Al-doped and Al-Sn co-doped ZnO nanostructures", Ceramics International, 39(6), pp. 6497–6502, 2013.
https://doi.org/10.1016/j.ceramint.2013.01.081

[61] Aksoy, S., Caglar, Y.Y., Ilican, S., Caglar, M. "Sol-gel derived Li-Mg co-doped ZnO films: preparation and characterization via XRD, XPS, FESEM", Journal of Alloys and Compounds, 512(1), pp. 171–178, 2012.
https://doi.org/10.1016/j.jallcom.2011.09.058

[62] Talat-Mehrabad, J., khosravi, M., Modirshahla, N., Behnajady, M. A. "Sol-gel Preparation and Characterization of Ag and Mg Co-doped Nano TiO_2: Efficient Photocatalytic Degradation of C.I. Acid Red 27", Research on Chemical Intermediates, 42(2), pp. 595–609, 2016.
https://doi.org/10.1007/S11164-015-2044-Z

[63] Suwanboon, S. "Structural and Optical Properties of Nanocrystalline ZnO Powder from Sol-gel Method", Science Asia, 34, pp. 31–34, 2008.
https://doi.org/10.2306/scienceasia1513-1874.2008.34.031

[64] Patterson, A. L. "The Scherrer Formula for X-Ray Particle Size Determination", Physical Review Journals Archive, 56, pp. 978–982, 1939.
https://doi.org/10.1103/PhysRev.56.978

[65] Reza, W., Bahnemann, D., Muneer, M. "A Green Approach for Degradation of Organic Pollutants Using Rare Earth Metal Doped Bismuth Oxide", Catalysis Today, 300, pp. 89–98, 2018.
https://doi.org/10.1016/j.cattod.2017.07.029

[66] Vignesh, K., Rajarajan, M., Suganthi, A. "Visible Light Assisted Photocatalytic Performance of Ni and Th Co-doped ZnO Nanoparticles for the Degradation of Methylene Blue Dye", Journal of Industrial and Engineering Chemistry, 20(5), pp. 3826–3833, 2014.
https://doi.org/10.1016/J.Jiec.2013.12.086

[67] Mehta, S. K., Kumar, S., Chavdhary, S., Bhasin, K. K. "Nucleation and Growth of Surfactant Passivated CdS and HgS NPs: Time Dependent Absorption and Luminescence Profiles", Supplementary Material for Nanoscale, Royal Society of Chemistry, 2, pp. 145–152, 2010.
https://doi.org/10.1039/B9NR00070D

[68] Evingur, G. A., Pekcan, O. "Optical Energy Band Gap of PAAm-GO Composites", Composite Structures, 183, pp. 212–215, 2018.
https://doi.org/10.1016/j.compstruct.2017.02.058

[69] Chand, P., Gaur, A., Kumar, A. "Structural and Optical Properties of ZnO Nanoparticles Synthesizes at Different pH Values", Journal of Alloys and Compounds, 539, pp. 174–178, 2012.
https://doi.org/10.1016/j.jallcom.2012.05.104

[70] Feroz, A. M. "Transparent Wide Band Gap Crystals Follow Indirect Allowed Transition and Bipolaron Hopping Mechanism", Results in Physics, 4, pp.103–104, 2014.
https://doi.org/10.1016/j.rinp.2014.06.001

[71] Wang, J., Gao, L. "Photoluminescence Properties of Nanocrystalline ZnO Ceramics Prepared by Pressureless Sintering and Spark Plasma Sintering", Journal of the American Ceramic Society, 88(6), pp. 1637–1639, 2005.
https://doi.org/10.1111/j.1551-2916.2005.00259.x

[72] Shirdel, B., Behnajady, M. A. "Sol-gel Synthesis of Ba-doped ZnO Nanoparticles with Enhanced Photocatalytic Activity in Degrading Rhodamine B under UV-A Irradiation", International Journal for Light and Electron Optics, 147, pp. 143–150, 2017.
https://doi.org/10.1016/j.ijleo.2017.08.059

[73] Mahyar, A., Behnajady, M. A., Modirshahla, N. "Characterization and Photocatalytic Activity of SiO_2-TiO_2 Mixed Oxide Nanoparticles Prepared by Sol-gel Method", Indian Journal of Chemistry, 49(12), pp. 1593–1600, 2010. [online] Available at: https://pdfs.semanticscholar.org/9220/7f72500895fc1b79bbfc495ac83abaabc12f.pdf [Accessed: 07 August 2018]

[74] Mahmoudi, E., Behnajady, M. A. "Synthesis of Fe_3O_4NiO Core-Shell Nanocomposite by the Precipitation Method and Investigation of Cr(VI) Adsorption Efficiency", Colloids and Surfaces A: Physicochemical and Engineering Aspects, 538, pp. 287–296, 2018.
https://doi.org/10.1016/j.colsurfa.2017.11.020

[75] Talat-Mehrabad, J., Khosravi, M., Modirshahla, N., Behnajady, M. A. "Synthesis, Characterization, and Photocatalytic Activity of co-Doped Ag-, Mg-TiO_2-P25 by Photodeposition and Impregnation Methods", Desalination and Water Treatment, 57(22), pp. 1–11, 2015.
https://doi.org/10.1080/19443994.2015.1036780

[76] Chakma, S., Moholkar, V. S. "Investigation in Mechanistic Issues of Sonocatalysis and Sonophotocatalysis Using Pure and Doped Photocatalysts", Ultrasonics Sonochemistry, 22, pp. 287–299, 2015.
https://doi.org/10.1016/j.ultsonch.2014.06.008

[77] Jia, T., Wang, W., Long, F., Fu, Z., Wang, H., Zhang, Q. "Fabrication, Characterization and Photocatalytic Activity of La-doped ZnO Nanowires", Journal of Alloys and Compounds, 484(1-2), pp. 410–415, 2009.
https://doi.org/10.1016/j.jallcom.2009.04.153

[78] Oppong, S. O-B., Anku, W. W., Opoku, F., Shukla, S. K., Govender, P. P. "Photodegradation of Eosin Yellow Dye in Water under Simulated Solar Light Irradiation Using La-Doped ZnO Nanostructure Decorated on Graphene Oxide as an Advanced Photocatalyst", Materials Science inc. Nanomaterials and Polymers, 3(4), pp. 1180–1188, 2018.
https://doi.org/10.1002/slct.201702470

[79] Xue, L., Xaing, L., Ting, L. P., Wang, C. X., Ying, L., Bao, C. C. "Mg Doping Reduced Full Width at Half Maximum of the Near-band-edge Emission in Mg Doped ZnO Films", Chinese Physics B, 19(2), ID: 027202, 2010.
https://doi.org/10.1088/1674-1056/19/2/027202

[80] Prabu, H. J., Johnson, I. "Greener Cum Chemical Synthesis and Characterization of Mg Doped ZnS Nanoparticles and their Engineering Band Gap Performance", Journal of Engineering Research and Application, 5(8), pp. 99–105, 2015. [online] Available at: http://www.ijera.com/papers/Vol5_issue8/Part%20-%204/M580499105.pdf [Accessed: 07 August 2018]

[81] Behnajady, M. A., Eskandarloo, H. "Characterization and Photocatalytic Activity of Ag-Cu/TiO_2 Nanoparticles Prepared by Sol-gel Method", Journal of Nanoscience and Nanotechnology, 13(1), pp. 548–553, 2013.
https://doi.org/10.1166/jnn.2013.6859

[82] Shakir, M., Faraz, M., Sherwani, M. A., Al-Resayes, S. I. "Photocatalytic Degradation of the Paracetamol Drug Using Lanthanum Doped ZnO Nanoparticles and them in-Vitro Cytotoxicity Assay", Journal of Luminescence, 176, pp. 159–167, 2016.
https://doi.org/10.1016/j.jlumin.2016.03.027

[83] Tayade, R. J., Kulkarni, R. G., Jasra, R. V. "Transition Metal Ion Impregnated Mesoporous TiO_2 for Photocatalytic Degradation of Organic Contaminants in Water", Industrial & Engineering Chemistry Research, 45(15), pp. 5231–5238, 2006.
https://doi.org/10.1021/ie051362o